Observation of grain size limited dynamic failure in a typical granite

SS Kirk[a,1], CH Braithwaite[a,*], AP Jardine[a] and DM Williamson[a]

[a]*Cavendish Laboratory, JJ Thomson Avenue, Cambridge, CB3 0HE, United Kingdom*

ABSTRACT

Understanding the dynamic fragmentation of geological materials is important to many fields, but is particularly significant for mining. Here, a series of expanding ring experiments are reported, investigating the dynamic fragmentation of a typical granite from a mining environment. In addition to in-situ diagnostics which measure time-resolved loading characteristics, fragments were soft-captured and analysed. Measured fragment size distributions agree well with existing theory, but show unexpected strain rate variation. Specifically, the reduction in fragment size with rate is shown to be limited as the fragments neared the material grain size, a phenomenon not previously observed. Inter-granular failure was confirmed by fractographic analysis of the recovered material. The phenomenon was hypothesised to be caused by the fragmentation being dominated by an intergranular fracture mechanism which becomes inhibited when fragments near the grain size. More generally, the approach provides a new experimental route through which the fragmentation of geological materials can be understood.

1. Introduction

Understanding the failure of geological materials is of fundamental importance to fields as diverse as civil engineering and interplanetary impact [1–3]. While quasi-static strength and toughness characteristics are relatively well understood [4], the high strain rate properties of geological materials remain poorly described. In particular, understanding the dynamic failure and fragmentation of different types of rock is vitally important to the mining industry, as it underpins the blasting process. Vast amounts of energy are used in post-blast comminution [2], so given the scale of the industry, even modest improvements in efficiency through better scientific understanding can result in significant reductions in energy usage. However, despite the importance of high-rate failure, accurate characterisation of dynamic rock processes remains a challenging problem. The wide range of strain rates involved makes small scale experiments difficult; in the region close to the centre of a blasthole, rates approach 104 s^{-1}, but drop away rapidly with distance [2]. In contrast, applying precise diagnostics to full-scale mining operations is extremely costly. The situation is further complicated by the multi-scale inhomogeneity of geological materials, necessitating extensive material characterisation. In this paper, we describe a series of laboratory-scale experiments that study the high-rate loading of a typical granite, revealing the dominance of microstructure in controlling macroscopic response. We use 'Lake Quarry Granite' (LQG) a well characterised Australian granite typical of a mining environment, composed of 74.8 ± 1.1 % orthoclase and 25.2 ± 1.1 % bronzite. Thin ring-shaped samples were loaded in a radial geometry, which causes circumferential tension. The tension causes cracks to grow across the ring and results in fragments being formed. The geometry provides a simple analogue for a blasthole, yet

given the specific strain rate, can be analysed using existing ring-fragmentation theory. We show that the reduction in fragment size with increasing rate becomes limited by the grain size of the material, which is of fundamental importance in developing realistic constitutive models.

2. Background

The brittle nature of geological materials means that, when dynamically loaded, they generally fracture in several places producing multiple fragments of different sizes and shapes [5]. A variety of alternative methods exist for studying dynamic fracture including Hopkinson bars [6–8] and spall experiments [9] and cylinder expansion experiments [10] in gas guns. However an expanding ring experiment has some advantages over these methods, in general being of a higher strain rate than Hopkinson bars and easier to recover fragments than in gas guns. There is also a fundamental advantage in that the geometrical arrangement of the experiment is much closer to that found in the application, and the loading pulse shape is correct. An explosive loading produces a Taylor wave loading profile [11] which is difficult to replicate precisely in non explosive loading environments. Other methods such as cratering [12] are also used, but are not so easily analyzed in terms of the results. The method proposed here is simple, replicates the real-world geometry and loading, is able to be conducted safely in a laboratory environment and also allows for multiple time resolved diagnostic methods to be employed. Geometric, empirical and physical models have been developed to predict the fragment size distribution (FSD) produced by rings. Geometric models are based on a body being geometrically divided in a random manner [13]. Simple empirical forms for the FSD have also been suggested based on experimental results [13]. Physical models are generally based on the relative rate of the expansion of the ring and the propagation speed of release waves emanating from the fracture surfaces, referred to in the literature as 'Mott release waves' [13–15]. These Mott waves propagate around the ring, relaxing the material and stopping further crack growth [15]. Higher strain rates cause

---

*Corresponding author

✉ chb32@cam.ac.uk (C. Braithwaite)

ORCID(s):

[1]Now at UKAEA, Culham Science Centre, Abingdon, Oxon, OX14 3DB, United Kingdom.
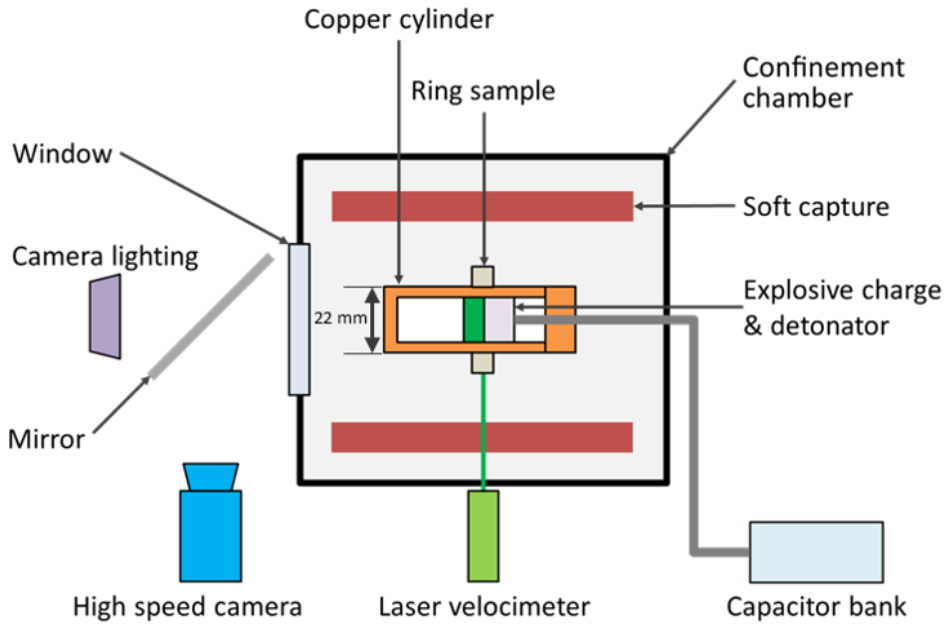
Figure 1: Schematic of the expanding ring experimental apparatus. Dynamic loading of the ring sample was provided by the copper cylinder containing a small explosive charge. The experiments were instrumented using high speed photography, laser velocimetry and soft capture.

greater circumferential stresses before relaxation, which in turn cause more cracks to initiate and grow [15–17]. The speed of the Mott waves remains constant, so increasing the strain rate produces smaller fragments. The most relevant physical model to geological materials is the elastic Mott model [15] which assumes the material remains elastic on both loading and release. Previous studies have shown the model agrees well with experiments [13–15,18–23]. The elastic Mott model predicts the fragment probability density function, $f(l)$, to be [13].

$$f(l) = \frac{4}{l_0 \sqrt{\pi}} e^{-\left(\frac{l}{l_0}\right)^2} erf\left(\frac{l}{l_0}\right) \qquad (1)$$

where l is the fragment length and l_0 is a length scale parameter defined by

$$l_0 = \sqrt{\frac{2\sigma c}{\dot{\epsilon}}} \qquad (2)$$

where σ is related to the initial crack distribution, c is the elastic sound speed and $\dot{\epsilon}$ is the strain rate.

Both geometric and empirical fragmentation models are useful mathematical functions to fit to FSDs, but they do not describe strain rate variation or consider microstructure. The physical models do include strain rate variation, but neglect microstucture by assuming a continuum material. Grain structure is a key parameter for geological materials, so experimental data demonstrating its effect is essential for understand the fragmentation process and the development of new models.

3. Experimental Methods

Expanding ring experiments are a well-established technique for studying the dynamic fragmentation of metals [13–15,18–24], which have been applied, though much less frequently, to ceramics [20], plastics [25], but not geological materials. Similar experiments (cylinders rather than rings) are also used to examine similar material behaviour for example [26,27]. The expanding ring apparatus used here, shown schematically in figure 1, consisted of a hollow copper cylinder containing an explosive charge, which radially loads a sample ring mounted on the outside. Ring samples (ID 22.29 ± 0.05 mm, OD 30.53 ± 0.05 mm, thickness 4.16 ± 0.16 mm) were cut from bulk LQG using diamond-tooling to give a square cross-section of 4.2 × 4.2 mm with sides parallel to within 0.1°. The average grain size was 0.45 mm, giving approximately 10 grains through the ring. The explosive charges each consisted of a Teledyne Risi RP-501 electric bridge-wire detonator and varying masses (nominally 0, 0.2, 0.5 and 0.7 grams) of Primasheet 1000 C3, to generate several different loading intensities and strain rates. A series of eight experiments were performed, with two repetitions at each of the four different loadings, inside a steel confinement chamber with a 30 mm thick polycarbonate window.

A series of diagnostics were deployed to follow the experiments. An Invisible Vision UHSi 12-24 framing camera with a 500 mm focal length mirror lens was used to observe a section of the ring (0.5µs exposure and 1µs interframe time). The sample was front-lit using flash lamps as shown, and the side face of the sample was coated with a thin layer of white paint to improve contrast (the coating was thin and weak compared to the rock, so did not affect the fragmentation).

The expansion velocity profile of the external ring surface was measured using a 1 mm diameter spot size heterodyne laser velocimeter (Het-V)[28], operating at 1550 nm and sampling at 2 GHz. A 16384 points (819 ns) Fourier transform window length was used in the analysis[28] to convert the output into velocity profiles. From the expansion velocity, the circumferential strain rate can be calculated using

$$\dot{\epsilon} = \frac{v}{r} \tag{3}$$

where v is the radial expansion velocity and r is the outer radius of the ring. The outer ring surfaces were also coated with a thin layer of retro-reflective paint to improve the Het-V signal.

The ring assembly was surrounded by a 25 mm thick layer of 1000 Mn polyethylene-glycol, cast inside a 150 mm diameter steel tube, to soft capture the granite ring fragments. Post experiment, fragments were recovered from the capture media by hot vacuum filtration at 80 ºC. FSDs were measured by sieving and weighing the recovered fragments, binning the results into sieve-pass intervals of 0-140, 140-250, 250-300, 300-560, 560-710, 710-1000, 1000-2000, 2000-3150 and 3150-6000 μm. For comparison with these results, the probability density function for a particular model can be converted into the cumulative mass fraction distribution, $F_m(l)$. Assuming the ring only fractures radially, the mass of a fragment, m, is related through $m \propto l$ and the cumulative mass fraction distribution is given by

$$F_m(l) = \frac{\int_0^l x f(x) dx}{\int_0^\infty x f(x) dx} \tag{4}$$

For the elastic Mott fragmentation model [1], the cumulative mass fraction distribution is:

$$F_m(l) = \frac{1}{1 + \frac{\sqrt{\pi}}{2} e^{\frac{1}{4}} \left(1 - erf\left(\frac{1}{2}\right)\right)}$$
$$\left\{1 - \frac{\sqrt{\pi}}{2} e^{\frac{1}{4}} erf\left(\frac{1}{2}\right)\right.$$
$$- e^{-\frac{l}{l_0}\left(1 + \frac{l}{l_0}\right)} \tag{5}$$
$$+ \frac{\sqrt{\pi}}{2} e^{\frac{1}{4}} erf\left(\frac{l}{l_0} + \frac{1}{2}\right)$$
$$\left. - \sqrt{\pi} e^{-\frac{l}{l_0}} \left(1 + \frac{l}{l_o}\right) erf\left(\frac{l}{l_0}\right)\right\}$$

which was fitted to the measured FSDs to obtain the length scale parameter for each experiment.

4. Results and Analysis

A typical high speed photographic sequence is shown in figure 2. The sample begins as a solid ring; as loading progresses, cracks initiate at the outside and grow through
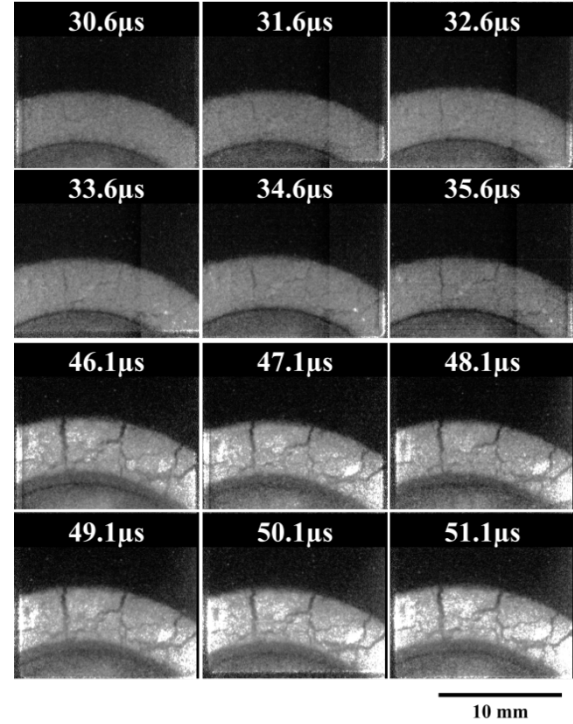

Figure 2: High speed photographic image sequence of a section of the ring from experiment 1 [Xing et al. 2017]. The time above each image denotes the time since initiation of the detonator. The ring sample can be seen to stretch, fracture radially and move outwards as distinct fragments.

the material. The cracks continue to grow until they reach the edges of the ring, separating into free fragments, which move out radially. The fracture pattern within the rings can be seen in the final image of figure 2; the cracks on the outer surface are equally spaced and aligned radially, whereas cracks on the inner surface are diagonally aligned. Ring fragmentation models generally assume radial cracking, indicating the limitations of current theory, and are a potential source of discrepancy.

Figure 3 shows a typical expansion velocity profile, extracted from the Het V measurements. The radial velocity rises rapidly to a peak, due to the arrival of the loading wave, which then reduces slightly as the ring stretches. The subsequent constant velocity plateau corresponds to the fragments having separated and being in free flight, leading to Mott waves which have relaxed the tension in the ring. The plateau start, indicating the arrival of the Mott waves, coincided with the onset of the fractures being observed with high speed photography. Peak expansion velocities were used to calculate the circumferential strain rate in each experiment (using equation 3), summarised in Table 1. No strain rate was recorded for experiment 8 due to recording error.

A typical mass distribution for the soft captured fragments is shown in figure 4, fitted by the elastic Mott model (equation 5). The model is in good agreement with the data, indicated by the high coefficients of determination (CoD) in Table 1, and allows the characteristic fragment length scales, l_0, to be
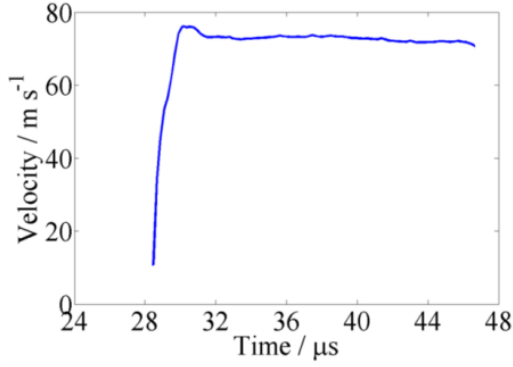
Figure 3: HExpansion velocity profile from experiment 3. The expansion velocity rises rapidly to a peak during loading, then reduces as the ring stretches, followed by a constant velocity plateau where the fragment is in free flight.
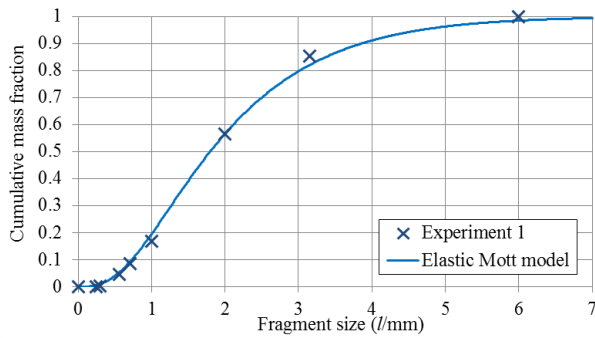

Figure 4: Cumulative mass fraction distribution from experiment 1 and fitted elastic Mott fragmentation model. The shape of the model agrees well with the experiment.

extracted, also summarised in Table 1. For comparison, the grain size of the original LQG was measured from a series of micrographs[29], averaging over 452 grains. The elastic Mott model was also fitted to that grain size distribution, giving $l_0 = 0.19 \pm 0.03$ mm with a CoD of 0.959.

Table 1
Length scale parameters and coefficients of determination from the fitted elastic Mott fragmentation models and measured strain rates of the expanding ring experiments.

Expt.	Strain rate ($\dot{\epsilon}/10^{-3}$ s^{-1})	Length scale parameter (l_o/mm)	Coefficient of determination (R^2)
1	3.96 ± 0.09	0.95 ± 0.04	0.998
2	2.93 ± 0.03	1.6 ± 0.2	0.970
3	4.98 ± 0.07	0.55 ± 0.02	0.999
4	5.58 ± 0.04	0.27 ± 0.04	0.966
5	8.05 ± 0.10	0.37 ± 0.07	0.986
6	6.58 ± 0.04	0.25 ± 0.02	0.991
7	6.64 ± 0.04	0.24 ± 0.03	0.977
8	-	0.35 ± 0.04	0.985

Figure 5 shows the variation in fragmentation length scale,

l_0, with strain rate (points), compared to the length scale parameter of the grains (horizontal dotted line). Initially, l_0 reduces roughly linearly with strain rate, following the expected behaviour. However, as the strain rate approaches approximately 5.5×10^3 s^{-1}, the fragment sizes stop reducing and remain broadly constant. This unexpected phenomenon corresponds to the point at which l_0 nears the grain size of the material.

Optical microscopy of a fragment, showed in Figure 6, demonstrates that although there are rough fracture surfaces, the fracture occurs around individual grain boundaries. Approaching a constant fragment size at high strain rates is inconsistent with existing theories, which generally predict that fragment sizes should continue to reduce. In fact, the initial reduction in fragment size we observe is much faster than predicted by equation 2. The dynamic resistance of a material can be described by fragmentation toughness,

$$K_f = \sqrt{\frac{1}{12}\rho c \dot{\epsilon} x_0^{\frac{3}{2}}} \tag{6}$$

where K_f is defined in analogy to fracture toughness, x_0 is the nominal fragment length and ρ is the bulk density[13]. Figure 6 shows the experimental data from Table 1 and the smooth interpolation converted to toughness using equation 6. K_f normally increases slowly with rate (i.e. equations 2 and 6), however in this case we see a rapid fall, followed by a leveling off around the point where the fragment size approached the grain size. The complex variation in toughness further demonstrates the experimental results do not agree with the existing fragmentation theory and new models are required.

5. Conclusions

The expanding ring technique was successfully applied to characterise the high strain rate tensile response of a typical granite, and was compared with the behaviour expected from existing theory. The distribution from the elastic Mott model was in good agreement with the measured FSDs, but showed an unexpected strain rate dependence; fragment sizes reduced with rate until a point, after which they remained constant. This discontinuity point coincided when the fragment size neared the original grain size of the material. It is hypothesised that this phenomena, which has not previously been observed, is caused by the fragmentation process being dominated by intergranular failure; initially the increasing stain rate causes greater tensile stresses in the ring which results in small fragments, as predicted by current fragmentation theory, but at the discontinuity point the material reaches complete intergranular fragmentation, where the material has disintegrated into into single grains, and the fragments cannot reduce any further without activating an intragranular fracture mechanism.

Optical microscopy of the fragments confirmed the fracture occurred at grain boundaries which gave credence to the proposed hypothesis. However, further experimental data is
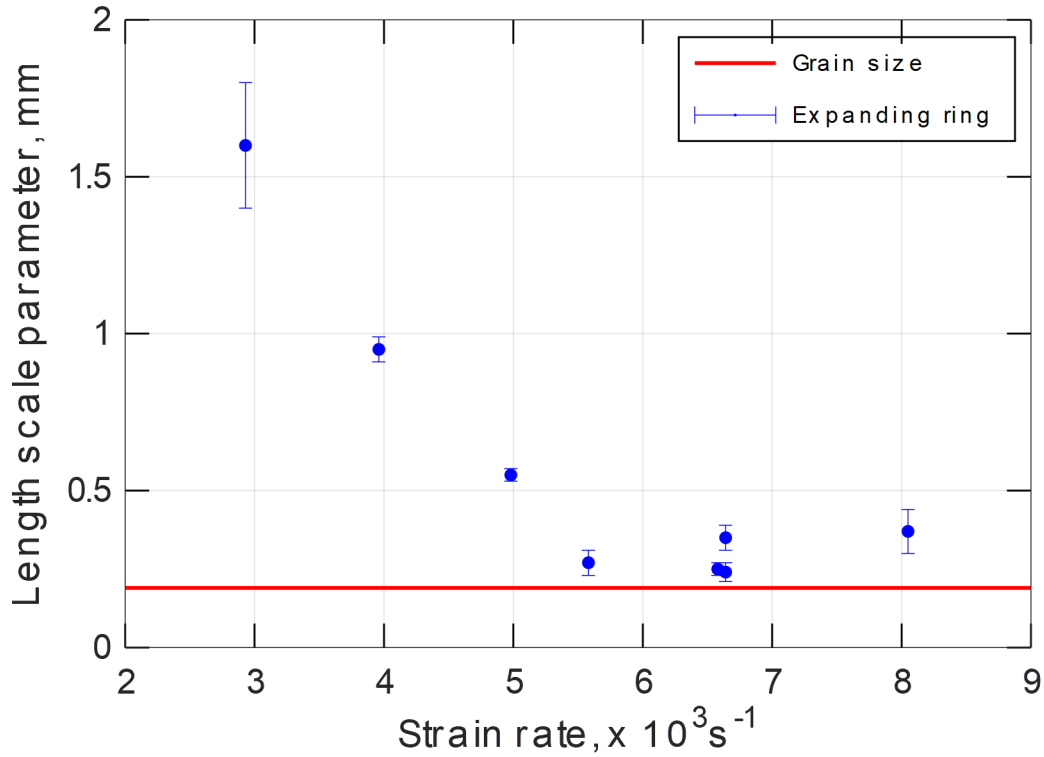
Figure 5: Variation in the length scale parameter with strain rate from the expanding ring experiments. The grain size of the original material has been added for reference. The length scale parameter of the recovered fragments reduces with strain rate, until it reaches the grain size, after which point it remains constant. The solid blue line is an interpolation to guide the eye.
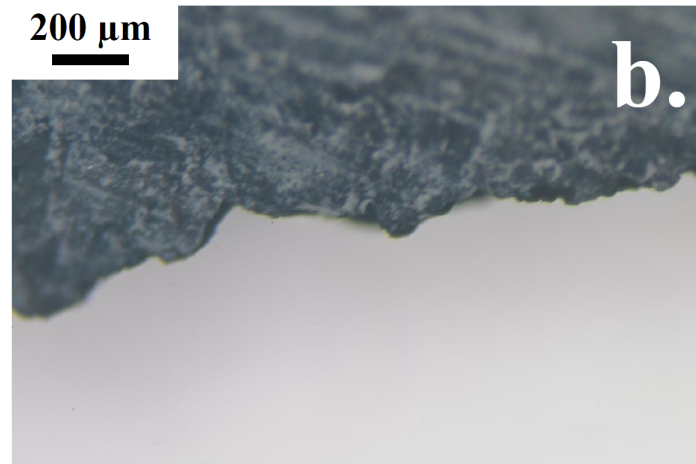

Figure 6: Optical microscope side-view image of fracture surface of a large fragment from Experiment 3. The edge is rough and the peak spacing of the roughness is on a similar scale to the grain size, 450 μm, which suggest intergranular fracture.

needed to confirm this hypothesis and could be achieved by a series of expanding ring experiments on geological materials of varying grain size.

References

[1] Feng, X.T., Hudson, J.A.. Rock engineering design. CRC Press; 2011.

[2] Hustrulid, W.A.. Blasting principles for open pit mining: general design concepts. Balkema; 1999.

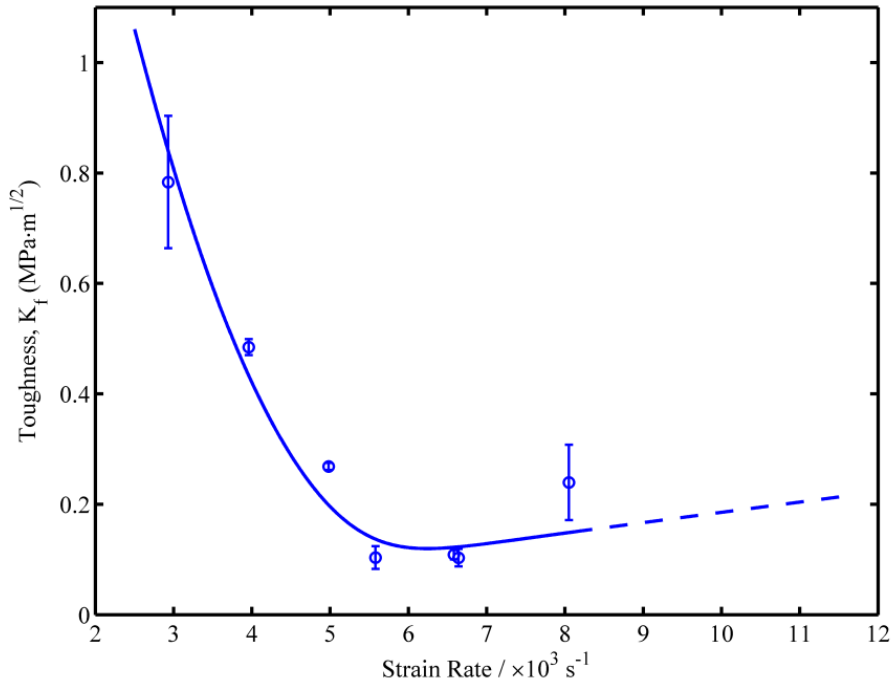[3] Leinhardt, Z.M., Stewart, S.T.. Collisions between gravity-dominated

Figure 7: Variation in fragmentation toughness, K_f, with strain rate. The toughness drops much more rapidly than expected from equations 2 and 6, before reaching a minimum and rising slowly as a result of the constant fragment size.

bodies. i. outcome regimes and scaling laws. The Astrophysical Journal 2011;745(1):79.

[4] Zhang, Q.B., Zhao, J.. A review of dynamic experimental techniques and mechanical behaviour of rock materials. Rock mechanics and rock engineering 2014;47(4):1411–1478.

[5] Lawn, B.. Fracture of brittle solids. Cambridge university press; 1993.

[6] Church, Philip, , Reynolds, Mark, , Gould, Peter, , Oakley, Robin, , Harrison, Nigel, , Williamson, Dave, , et al. Tensile properties of am maraging steel. EPJ Web Conf 2018;183:01058. URL: https://doi.org/10.1051/epjconf/201818301058. doi:10.1051/epjconf/201818301058.

[7] Wong, L.N.Y., Li, Z., Kang, H.M., Teh, C.I.. Dynamic loading of carrara marble in a heated state. Rock Mechanics and Rock Engineering 2017;50(6):1487–1505. URL: https://doi.org/10.1007/s00603-017-1170-x. doi:10.1007/s00603-017-1170-x.

[8] Xu, Y., Dai, F.. Dynamic response and failure mechanism of brittle rocks under combined compression-shear loading experiments. Rock Mechanics and Rock Engineering 2018;51(3):747–764. URL: https://doi.org/10.1007/s00603-017-1364-2. doi:10.1007/s00603-017-1364-2.

[9] Field, J.E., Braithwaite, C.H., Guest, A.R., Proud, W.G.. Investigations into the spall strengths of geological materials. AIP Conference Proceedings 2007;955(1):1375–1378. URL: https://aip.scitation.org/doi/abs/10.1063/1.2832980. doi:10.1063/1.2832980. arXiv:https://aip.scitation.org/doi/pdf/10.1063/1.2832980.

[10] Jones, D.R., Chapman, D.J., Eakins, D.E.. A gas gun based technique for studying the role of temperature in dynamic fracture and fragmentation. Journal of Applied Physics 2013;114(17):173508. URL: https://doi.org/10.1063/1.4828867. doi:10.1063/1.4828867. arXiv:https://doi.org/10.1063/1.4828867.

[11] Hixson, R.S., Gray, G.T., Rigg, P.A., Addessio, L.B., Yablinsky, C.A.. Dynamic damage investigations using triangular waves. AIP Conference Proceedings 2004;706(1):469–472. URL: https://aip.scitation.org/doi/abs/10.1063/1.1780279. doi:10.1063/1.1780279. arXiv:https://aip.scitation.org/doi/pdf/10.1063/1.1780279.

[12] Zhang, F., Peng, J., Qiu, Z., Chen, Q., Li, Y., Liu, J.. Rock-like brittle material fragmentation under cou-

pled static stress and spherical charge explosion. Engineering Geology 2017;220:266 – 273. URL: http://www.sciencedirect.com/science/article/pii/S0013795216303003. doi:https://doi.org/10.1016/j.enggeo.2017.02.016.

[13] Grady, D.. Fragmentation of rings and shells: the legacy of NF Mott. Springer Science & Business Media; 2007.

[14] Grady, D., Benson, D.. Fragmentation of metal rings by electromagnetic loading. Experimental Mechanics 1983;23(4):393–400.

[15] Mott, N.F.. Fragmentation of shell cases. Proceedings of the Royal Society of London Series A Mathematical and physical sciences 1947;189(1018):300–308.

[16] Anderson, T., Anderson, T.. Fracture mechanics: fundamentals and applications. 2005. Boca Raton, Fla: Taylor & Francis 2005;.

[17] Griffith, A.A.. Vi. the phenomena of rupture and flow in solids. Philosophical transactions of the royal society of london Series A, containing papers of a mathematical or physical character 1921;221(582-593):163–198.

[18] Hiroe, T., Fujiwara, K., Hata, H., Takahashi, H.. Deformation and fragmentation behaviour of exploded metal cylinders and the effects of wall materials, configuration, explosive energy and initiated locations. International Journal of Impact Engineering 2008;35(12):1578–1586.

[19] Hoggatt, C., Recht, R.. Stress-strain data obtained at high rates using an expanding ring. Experimental Mechanics 1969;9(10):441–448.

[20] Levy, S., Molinari, J.F., Vicari, I., Davison, A.. Dynamic fragmentation of a ring: Predictable fragment mass distributions. Physical Review E 2010;82(6):066105.

[21] Martineau, R., Anderson, C., Smith, F.. Expansion of cylindrical shells subjected to internal explosive detonations. Experimental Mechanics 2000;40(2):219–225.

[22] Xue, Q., Meyers, M., Nesterenko, V.. Self-organization of shear bands in titanium and ti–6al–4v alloy. Acta Materialia 2002;50(3):575–596.

[23] Zhou, F., Molinari, J.F., Ramesh, K.. Analysis of the brittle fragmentation of an expanding ring. Computational Materials Science 2006;37(1-2):74–85.

[24] Marquez, A.M., Braithwaite, C.H., Weihs, T.P., Krywopusk, N.M., Gibbins, D.J., Vecchio, K.S., et al. Fragmentation and constitutive response of tailored mesostructured aluminum compacts. Journal of Applied Physics 2016;119(14):145903. URL: https://doi.org/10.1063/1.4945813. doi:10.1063/1.4945813. arXiv:https://doi.org/10.1063/1.4945813.

[25] Zhang, Jia, , Zheng, Yuxuan, , Zhou, Fenghua, , Liu, Jun, . Experimental technique for dynamic fragmentation of liquid-driving expanding ring. EPJ Web Conf 2018;183:02034. URL: https://doi.org/10.1051/epjconf/201818302034. doi:10.1051/epjconf/201818302034.

[26] Balagansky, I.A., Vinogradov, A.V., Merzhievsky, L.A., Matrosov, A.D., Stadnichenko, I.A.. Effect of shell material on the detonation of an explosive charge. Combustion, Explosion, and Shock Waves 2018;54(4):502–510. URL: https://doi.org/10.1134/S0010508218040147. doi:10.1134/S0010508218040147.

[27] Jeong, H., Jeon, B., Choi, S., Jeon, S.. Fracturing behavior around a blasthole in a brittle material under blasting loading. International Journal of Impact Engineering 2020;140:103562. URL: http://www.sciencedirect.com/science/article/pii/S0734743X1930973X. doi:https://doi.org/10.1016/j.ijimpeng.2020.103562.

[28] Strand, O.T., Berzins, L.V., Goosman, D.R., Kuhlow, W.W., Sargis, P.D., Whitworth, T.L.. Velocimetry using heterodyne techniques. In: 26th International Congress on High-Speed Photography and Photonics; vol. 5580. International Society for Optics and Photonics; 2005, p. 593–599.

[29] Carter, R.M., Yan, Y.. Measurement of particle shape using digital imaging techniques. In: Journal of Physics: Conference Series; vol. 15. IOP Publishing; 2005, p. 177.